

Mixing Characteristics of Compressible Planar Mixing Layer Impinged by Oblique Shock Waves

By **B. Wang, S. Xue, H. Zhang, X. Y. Hu[†]** AND **N. A. Adams[†]**

School of Aerospace, Tsinghua University, Beijing China 100084

This paper mimics a spatially developing compressible planar mixing layer turbulent flow under the action of an oblique shock wave employing direct numerical simulation. The interaction of shock wave and large scale turbulent vortexes in the mixing layer is then investigated for the purpose of revealing the mixing characteristics. The large scale coherent vortexes are compressed by the oblique shock so that their vorticity is enhanced. The thickness of shocked mixing layer is firstly decreased due to the compressible effects of shock wave, and then increased, and finally exceeds that of shock-free mixing layer because of an increased thickness growth rate. The mixing efficiency of mixing layer is found to be intensified via analyzing the passive scalar transport in the mixing layer flow. The turbulent kinetic energy and velocity fluctuating levels are strengthened in shocked mixing layer flows. Analysis on physical mechanisms of enhancement of turbulence and mixing are also performed from aspects of production terms in Reynolds-stress transport equation and vortex dynamics equation.

1. Introduction

It is difficult to realize well mixing between fuels and airflows in the combustor of scramjet, because both airflows move beyond sonic speed, and the residing time of the airflows is very short, which is in the magnitude order of micro-second. Even if the mixing layer flow is employed in the combustor, the shear between airflows and injected fuel flows is more stable due to strong compressible effects of high-speed flow. Therefore, enhancing mixing is one of the key technologies for advancing the engine performance.

Recently, people have suggested different approaches to strengthen mixing in the supersonic combustor. A summary of them by Seiner [1] is reproduced in Tab. 1. The possible mixing enhancement approaches are classified into passive control and active control ones. As is shown in Tab. 1, the passive method via the interaction between oblique shock wave and mixing layer has provoked the widest range of readings. Complex shock waves are in the intake, isolator and combustor of scramjet. As one of the inherent flow structures in supersonic combustors, it is pretty economical and rational to utilize shock wave to promote the mixing of fuels and airflows.

Besides the solid backgrounds of practical applications in engineering, the interaction of shock wave and turbulent flows is also one of the most fundamental issues given rise to be researched. This complicated flow phenomena in supersonic flows contains

[†] Lehrstuhl für Aerodynamik und Strömungsmechanik, Technische Universität München, Boltzmannstr. 15, 85748 Garching b. München

Passive methods		Active methods	
Mixing devices	Physics mechanism	Mixing devices	Physics mechanism
Swept ramps / Tabs / Lobe mixers / Chevrons	Streamwise vortexes	Vibrating splitter / Wire	Large scale excited
Swirl	Streamwise vortexes	Pulsed jet	Large scale excited
Port geometry	Self-excited resonance	Helmholtz resonators	Large scale excited
Streamwise curvature	Effects of curvature	Piezoelectric actua- tors	Large scale excited
Shock / Shear layer interaction	Large-scale turbulence excited	Acoustic excitation	Large scale excited
Counterflow	Self-excited resonance	Wave wall	Large scale excited spatially
Backward- facing/multi-step	Self-excited resonance	Flip-flop nozzle	Increase of transverse curvature
Cavities	Self-excited resonance		

TABLE 1. Mixing enhancement methods in supersonic combustor.

linear and nonlinear physical mechanisms, which would result in significant variations of turbulent coherent structures and statistical properties, and correspondingly in a change of dynamics of shock waves.

Velocity fluctuations are found to be intensified in the study of interaction of shock and turbulence, which implies that turbulent mixing could be enhanced by the action of shock [2]. Mixing enhancement induced by external shocks was observed in the experiments performed by such as Marble *et al.* [3], Menon [4], and Budzinski *et al.* [5]. Hermanson *et al.* [6] carried through experimental studies on supersonic jets of different airflows of helium, air and carbon dioxide. They found that the concentration of helium airflow is lowered the most and its spatial distribution is uniformed interacted by shock waves; the degree of mixing enhancement is then increased more than 30%. However, for air and carbon dioxide airflows, there is no such evident enhancement of mixing. Shau *et al.* [7] also observed the phenomenon of mixing enhancement induced by shock waves, but they claimed that the intensifying effects only exist close to the shock wave and the mixing efficiency downstream recovers to that of undisturbed status. Although the above qualitative experiments confirmed that shock waves are able to intensify mixing of supersonic airflows, the physical mechanisms are yet to be investigated further.

Nuding *et al.* [8] considered effects of shock wave strength, shock wave impinging position and convection Mach number of mixing layer to perform the investigations on interactions of shock and planar mixing layer flows. They concluded that the stronger the shock wave is, and the mixing is better. They indicated that there are almost no effects on mixing efficiency changing the convection Mach number of mixing layer. Although they also tried to address that the mixing is better as the shock wave impinges downstream,

such the conclusion cannot be obtained based on the contradictory data presented in their paper. Drummond [9] numerically studied the interactions of jets and oblique shock waves and confirmed that the streamwise vorticity is increased by the shock and the mixing process is hence intensified. Lu and Wu [10] numerically studied the interactions of wall-bounded supersonic mixing layer flows with oblique shock waves. They indicated that mixing can be enhanced, only if the mixing layer flow is excited continually by shock wave as well as the shock wave acts on the mixing layer pretty close to the upstream of the flow. Kim *et al.* [11] performed a RANS simulation of a scramjet combustor and found that the growth rate of mixing layer thickness is largely raised after an interaction with the oblique shock wave, and hence the mixing efficiency is heightened. GÃn'in *et al.* [12] studied the shocked mixing layer flows by two oblique shock waves using large eddy simulation. They found that the turbulence fluctuating levels is enlarged and the mixing layer growth rate is increased as the interaction position moves downstream, but they also indicated that the mixing enhancement is localized around the action position of shock wave on the mixing layer. According to the research findings that turbulence fluctuating levels cannot be recovered downstream, they proposed that the increased growth rate of mixing layer is caused by the decreased convection Mach number of the shocked mixing layer.

Either the experimental or the numerical studies verified that the mixing can be intensified in a shocked mixing layer flow. However, few studies have been done on the complicated interaction of shock wave and turbulence, or that of shock wave and large scale coherent eddy structures. Few investigations support to well understand physics of mixing enhancement in mixing layer turbulent flows acted by oblique shock wave. Therefore, taking the spatially developing compressible mixing layer turbulent flow as the prototype flow in the scramjet combustor, we study the interaction of oblique shock wave and mixing layer by a direct numerical simulation to reveal physical mechanisms of mixing enhancement in this paper.

2. Numerical procedures

2.1. Governing equations

A direct numerical simulation is employed in the present study. The conserved Navier-Stokes equations in a Cartesian coordinates are written as, neglecting body force and external thermal sources,

$$\frac{\partial \rho}{\partial t} + \frac{\partial \rho u_j}{\partial x_j} = 0 \quad (2.1)$$

$$\frac{\partial \rho u_i}{\partial t} + \frac{(\partial \rho u_i u_j + p \delta_{ij})}{\partial x_j} = \frac{\partial \tau_{ij}}{\partial x_j} \quad (2.2)$$

$$\frac{\partial \rho E}{\partial t} + \frac{(\partial \rho E + p) u_j}{\partial x_j} = \frac{\partial (u_k \tau_{kj} + q_j)}{\partial x_j} \quad (2.3)$$

where $\tau_{ij} = \mu \left(\frac{\partial u_i}{\partial x_j} + \frac{\partial u_j}{\partial x_i} - \frac{2}{3} \frac{\partial u_k}{\partial x_k} \delta_{ij} \right)$ and $q_j = k \frac{\partial T}{\partial x_j}$.

Equations (2.1)-(2.3) are the continuity, momentum and total energy equations, respectively. x_j is the Cartesian coordinates; t is the time; ρ is the density; p is the pressure; E is the total energy per unit mass of gas. u_j are the velocity components in the j^{th} direction ($j = 1, 2, 3$); τ_{ij} are the viscous-stress; q_j are heat flux in the j^{th} direction. k is the gas thermal conductivity. The viscosity is calculated by the Sutherland formula

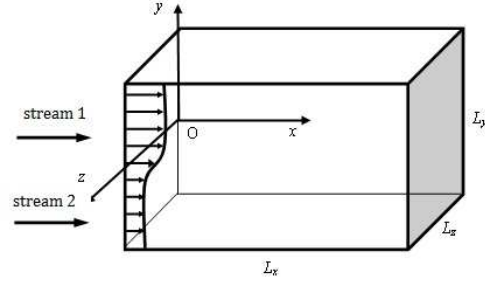


FIGURE 1. Calculation domain for the mixing layer flow.

Inflow	Outflow	Transverse 1	Transverse 2	Spanwise
Velocity profiles with instability disturbance	Supersonic extrapolation	Oblique shock wave relationship	Non-reflective	Periodicity

TABLE 2. Boundary conditions.

as,

$$\mu = \mu_{\infty} (T/T_{\infty})^{1.5} \left(1 + \frac{T_S}{T_{\infty}} \right) / \left(\frac{T}{T_{\infty}} + \frac{T_S}{T_{\infty}} \right) \quad (2.4)$$

where $T_S = 110.4K$, and μ_{∞} is the viscosity of free stream, and T_{∞} is the temperature of free stream. The above equations are closed by the gas state equation, denoting as

$$p = (\gamma - 1) \rho \left(E - \frac{u^2 + v^2 + w^2}{2} \right) \quad (2.5)$$

To study the mixing properties of the two streams, a passive scalar variable f is introduced and its transport equation is written as,

$$\frac{\partial(\rho f)}{\partial t} + \frac{\partial(\rho f u_j)}{\partial x_j} = -\frac{\partial}{\partial x_j} \left(-\rho D \frac{\partial f}{\partial x_j} \right) \quad (2.6)$$

where D is the mass diffusion coefficient of passive scalar, and it can be related with the fluid viscosity via Schmidt number, $Sc = \mu/\rho D$. In this paper, Sc is taken as 1 and Pr number is taken as 0.72.

2.2. Calculation domain and boundary conditions

Figure 1 shows the sketch of the physical model of spatially developing mixing layer flow and the calculation domain employed in the present simulation.

Because the intense coupling between the reflection of acoustic waves and turbulence is able to induce calculation instability and to influence the flow developing, the reflection of waves on the calculation domain boundaries must be removed strictly. Proper calculation boundary conditions are needed for solve compressible mixing layer turbulent flows. Table 2 shows the boundary conditions employed in the present simulation.

Here, the inflow mean velocity profile in the streamwise direction is specified as below,

$$u(y) = \frac{U_1 + U_2}{2} + \frac{U_1 - U_2}{2} \tanh\left(\frac{y}{2\delta_0}\right) \quad (2.7)$$

where U_1 and U_2 are the free-streamwise velocity for stream 1 and 2; δ_0 inlet momentum layer thickness. The inflow disturbance is taken as,

$$\begin{aligned} u(x=0, y, z) &= w(x=0, y, z) = 0 \\ v'(x=0, y, z) &= \Delta U G(y) A \sin(2\pi ft + \phi) \end{aligned} \quad (2.8)$$

Where f is the most unstable frequency; $G(y)$ is the Gaussian function; A is the amplitude; ϕ is the random phase difference.

2.3. Numerical discretization schemes

We employed a high-order hybrid scheme proposed by Ren *et al.* [13] for calculating non-viscous numerical flux. The scheme is hybridized a fifth-order WENO scheme, which dominates in the flow field with discontinuity, and a fifth-order compact scheme, which dominates in the smooth regions in the flow field, through a smooth indicator function. This scheme, based on the eigenvalue decomposition method, was successfully used for simulating compressible flow as well as mixing layer turbulent flows [14].

We use a sixth-order symmetric compact scheme for calculating viscous flux and a third order Runge-Kutta explicit scheme for the time integration.

2.4. Validation

For the order of validating the present numerical procedure, a shock-free mixing layer turbulent flow was simulated. The calculation parameters are the same as those in experiments conducted by Goebel *et al.* [15], where the thickness of mixing layer and velocity moments were measured.

Figure 2 shows the present numerical results of spatial evolution of mixing layer flow. The coherent structures are extracted by the second invariant of the velocity gradient, shown in Fig. 2(a) and also presented by the streamwise component of vorticity in Fig. 2(b). The developing process undergoes the initial instability (first instability), spanwise vortex rolling up, shedding, pairing and merging of vortices. Downstream, the spanwise vortexes experience curving, lifting, twisting, stretching and finally breaking up to small scale eddies, accompanying with the appearance of streamwise and transverse vortexes stimulated by the second instability waves.

The mixing layer develops to a similarity status in a linear way. The thickness of mixing layer is plotted in Fig. 3. The mixing layer linearly grows after $x/L_x > 0.7$. Fitting the numerical data, a mixing layer thickness growth rate is obtained as $B = d\delta(y)/dt = 0.022$ which is the same as the value experimentally measured.

The mean and fluctuating velocities together with Reynolds-stress are statistically obtained. They are compared with the experimental measurements in Fig. 4. The profiles are plotted with a variance of a self-similarity variable η . η is defined as,

$$\eta = \frac{y - y_{0.5}}{\delta} \quad (2.9)$$

There is a good self-similarity in the fully developed flow regions for the spatially developing mixing layer turbulent flow. For the present conditions, if $x/L_x > 0.7$, the flow reaches the self-similarity status. It is found that it is earlier to achieve the self-similarity

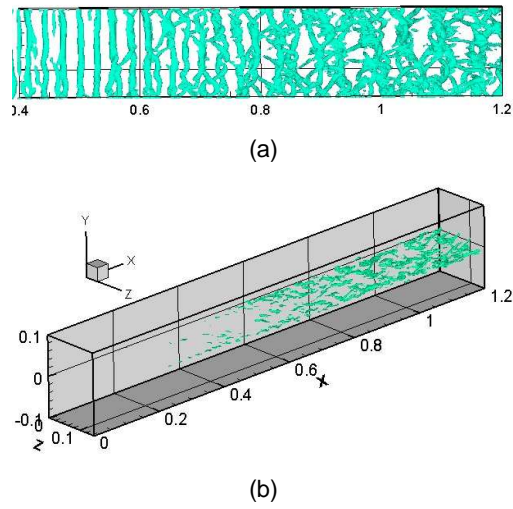


FIGURE 2. Spatially evolving of large scale coherent structures of mixing layer. (a) the second invariant of the velocity gradient $Q_2 = 10^7 s^{-2}$; (b) the streamwise vorticity $\omega_x = -10000 s^{-1}$.

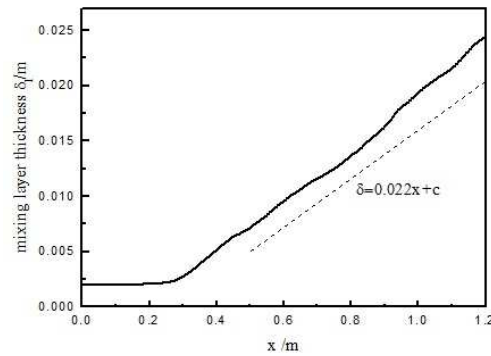


FIGURE 3. Mixing layer thickness.

for the first moment of velocity, i.e., the mean velocity in the streamwise direction, as shown in Fig. 4a. Although there are some differences between the numerical data and experimental measures, a good self-similarity can also be observed for the Reynolds-stress. The good agreements of numerical results with experimental data validate that the present numerical procedure is accurate and reliable.

3. Results and discussion

The oblique shock wave impinges from the up-stream 1 with the shock angle $\beta = 36^\circ$ with the strength $\Delta P/P_1 = 1.16$. The incident shock penetrates the mixing layer (both two streams) and is refracted due to the difference in the flow parameters.

The calculation domain is taken as $1.2m \times 0.6m \times 0.15m$. The grid resolution is $512 \times 256 \times 64$. The flow parameters are specified as $U_1 = 609.1m/s$, $M_1 = 2.4$; $U_2 = 456.8m/s$, $M_2 = 1.8$. Therefore, the convection Mach number Mc is taken as 0.3. The

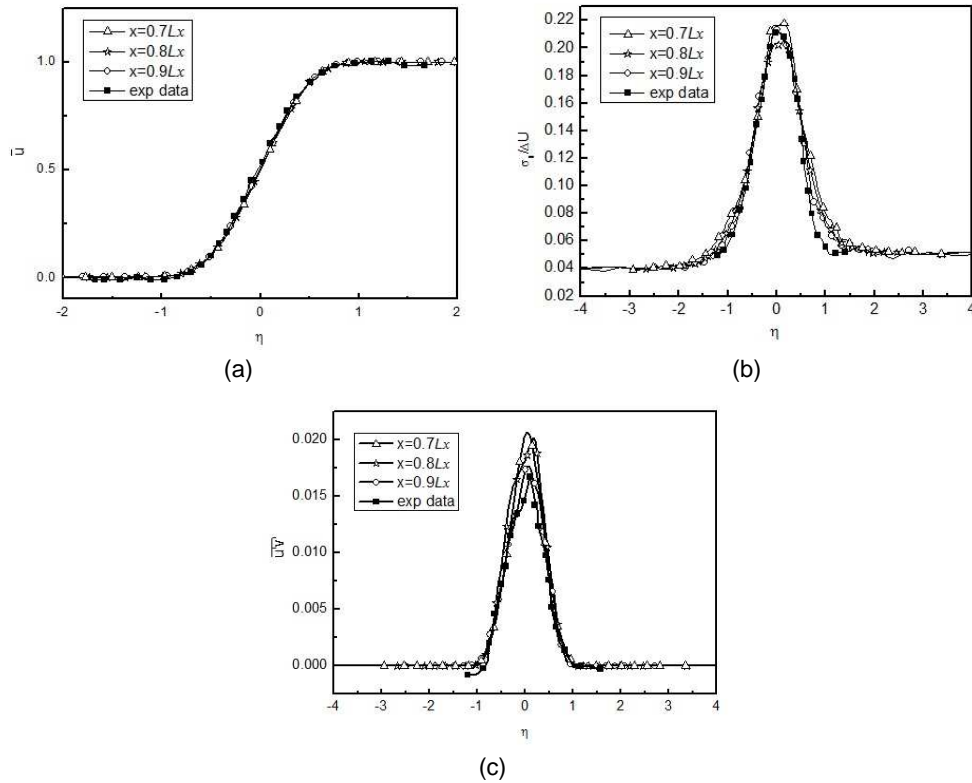


FIGURE 4. Comparisons of statistics of velocity moments. (a) mean velocity in the streamwise direction; (b) r.m.s velocity in the streamwise direction; (c) Reynolds-stress.

static pressure of both streams is equal to each other, i.e., $P_1 = P_2 = 46 \text{ kPa}$; the gas density is the same, taking as 1 kg/m^3 .

3.1. Large scale coherent structures

Large scale coherent structures are the most significant characteristics of compressible mixing layer flows. They dominate the transports of mass, momentum and energy of the mixing layer. The coherent structures in the mixing layer will respond to the interaction with the oblique shock wave.

Comparisons of large scale coherent structures' developments are shown in Fig. 5 for two cases without and with action of oblique shock wave. Here, the iso-contours of spanwise vorticity are employed. The airflows in the shocked mixing layer deflect towards the oblique shock wave front, as they pass through the shock wave. Therefore, from the flow pattern, the shocked mixing layer is inclined down due to the change of airflows direction.

Note that vortices are compressed in the normal direction of shock wave front downstream from the position of interaction point A between the incident shock wave and the mixing layer, and their vorticity are hence increased.

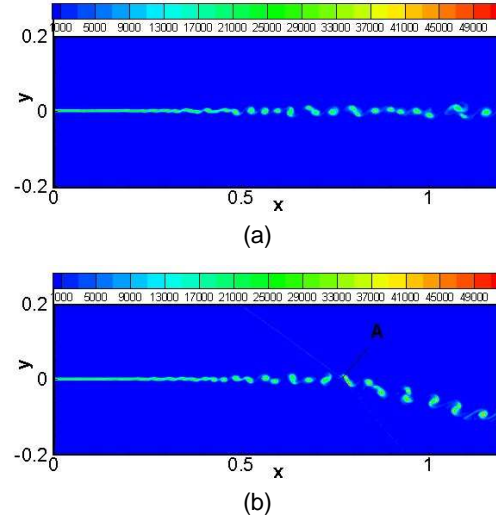


FIGURE 5. Iso-contours of spanwise vorticity. (a) shock-free mixing layer; (b) shocked mixing layer.

3.2. Shock wave structures

As is known that the oblique shock, acting on the mixing layer, will happen to reflect and refract because of the difference of stream properties. Moreover, the types of the reflection and refraction waves depend on the stream parameters. The following will present the analysis of shock wave structures.

The iso-contours of density or pressure cannot be utilized to clearly visualize evolutions of the sonic wave or weak waves. Therefore, the variable q_1 , which is very sensitive to the density gradient, is employed to better flow visualization of shock waves in the interacted flow fields. The iso-contour of variable q_1 is generally called as schlieren graph. In the present simulation, q_1 is calculated as,

$$q_1(x, y) = 0.8 \exp(-0.8q/q_{max}) \quad (3.1)$$

where $q(x, y) = \left(\frac{\partial \rho}{\partial x}\right)^2 + \left(\frac{\partial \rho}{\partial y}\right)^2$; q_{max} is the maximum value of q in the flow field considered. According to (3.1), q_1 is ranged from 0.36 to 0.8. In flow fields, the stronger the shock waves are, the larger the density gradients are. The value of q then approaches to q_{max} , and correspondingly, q_1 is taken as the value close to 0.36. In the smooth flow fields without discontinuity (shock waves), q approaches to zero and q_1 is taken as the value close to 0.8. Therefore, utilizing (3.1), the variations of density gradient are amplified. Meanwhile, the value of q_1 can be taken values in a small range, and it is better to clearly visualize weaker waves.

Figure 6 shows the schlieren photograph to present the shock wave structures in the shocked-mixing layer flow field. The shock wave structures commonly consists of incident shock (IS), infraction wave (TS) and reflection isentropic wave (RW), if the incident shock wave acts on mixing layer with different Mach number for the up- and downstream.

The type of reflection isentropic wave (RW) depends on the relative Mach number of both two streams. Buttsworth [16] analyzed that: if the incident shock wave impinges from the high Mach number side to the low Mach number side, it derives reflection isen-

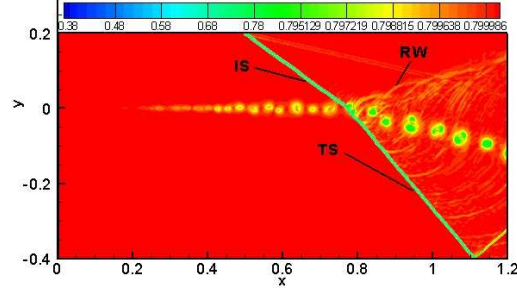


FIGURE 6. Schlieren photography of shock waves in the flow field. (IS is the incident shock wave; RW is the reflection isentropic expansion waves; TS is the infracation shock wave.

tropic expansion waves; if inversely, it derives reflection isentropic compression waves. In the present simulation, Mach number of up-stream is 2.4 and 2.8 for the down-stream. The incident shock wave is impinged from the up-side to the down-side, and therefore, the reflection waves are isentropic expansion ones. Figure 6 can also demonstrates that the static pressure behind the reflection waves is smaller than that in front of them.

The static pressure ratio behind and in front of a shock wave generally represents the strength of shock wave. In the present study, the static pressure of both two streams is the same in front of the incident shock wave, denoting as p_1 . For the up airstream, the pressure is increased as p_2 behind the IS shock wave, but it is then decreased as p_3 when the airflows pass through the reflection expansion waves. For the down airstream, the static pressure is increased as p_4 behind the refraction shock wave. Matching the condition of the airstreams, p_3 must be equal to p_4 . Hence, p_2 is larger than p_4 , and $p_2/p_1 > p_4/p_1$. The strength of infracation shock wave is therefore smaller than that of incident shock wave.

3.3. Mixing properties

We proposed a definition describing the mixing efficiency of fluid entrained in mixing layer,

$$\varepsilon_m(x) = \frac{4 \int_0^x \int_{\delta_1} \overline{\rho^2 f(1-f)} dy d\xi}{\int_0^x \int_{\delta_1} \overline{\rho^2} dy d\xi} \quad (3.2)$$

According to the definition, if the passive scalar f is 0.5 for the fluid entrained into the mixing layer, the mixing is the best, and the mixing efficiency is 1. If f is zero or unity, the mixing is the worst, and the mixing efficiency is 0. The definition states that the weights for fluid in their degree of mixing are different, i.e., in the center of the mixing layer, the weight for better mixed fluid is higher, whereas in the edge of mixing layer, the weight for worse mixed fluid is lower. Thus, the definition is not limited to boundaries, only taking into account the mixing levels of entrained fluid but not the free fluid outside mixing layer.

Figure 7 compare the thickness of mixing layer for cases with and without oblique shock wave. As the shock wave penetrates the mixing layer at point A, the mixing layer is locally compressed by the shock wave. The mixing layer thickness is decreased rapidly, corresponding to a “concave pit” in the curves. However, the growth rate of mixing layer thickness, $d\delta/dx$, is also increased by the shock, and therefore, the mixing layer accelerate grows thickly and the thickness of shocked mixing layer finally exceeds that without shock acting. At the outlet of the calculation domain, the thickness of shocked mixing layer is increased 11%.

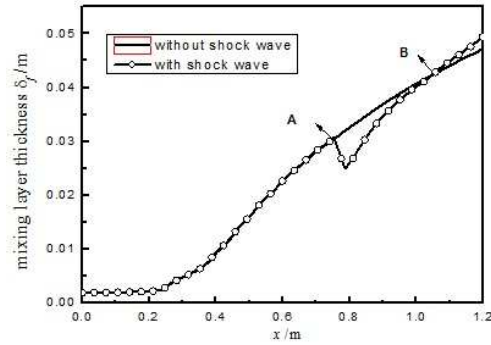


FIGURE 7. Comparisons of mixing layer thickness.

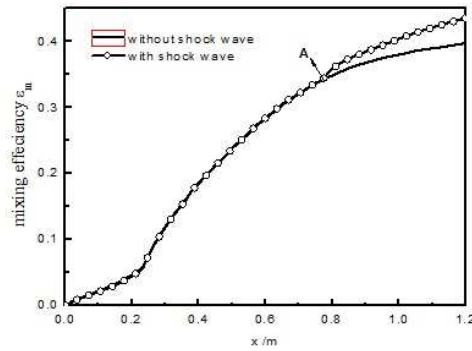


FIGURE 8. Comparisons of mixing efficiency.

The thickness of mixing layer can only indicate the entrainment quantity of free streams, but cannot demonstrate the mixing efficiency of two free streams. Figure 8 compares the mixing efficiency for mixing layer flow and shocked mixing layer flow. The mixing efficiency $\varepsilon_m(x)$ significantly increases when the flow is acted by a shock wave. It is shown the mixing efficiency is enhanced at the action point A and to the end of the calculation domain it is increased about 10%. The mixing efficiency is not increased as much as the thickness of mixing layer.

4. Conclusions

The spatially developing compressible mixing layer turbulent flows are numerically simulated under an action of oblique shock wave. The interaction of mixing layer and shock wave is then investigated to reveal the mixing layer enhancement from aspects of evolution of the turbulent coherent structures and shock waves. Turbulence statistics are also compared for two cases of shock-free and shocked mixing layer flows. It is then found that (1) Vortexes of mixing layer are compressed by shock wave and their vorticity are increased. (2) The thickness of shocked mixing layer is first decreased due to the compression impact of shock wave, but finally exceeds that of shock-free mixing layer due to a larger thickness growth rate. The mixing efficiency is hence heightened in the present of shock wave introduced.

References

- [1] SEINER, J. M., DASH, S. M. AND KENZAKOWSKI, D. C. (2001). History survey on enhanced mixing in scramjet engines. *J. Propulsion and Power*, **17**(6), 1273–1286.
- [2] YIANNIS, A., JUAN, H. A. AND GEORGE, B. (2000). Shock wave-turbulence interactions. *Annu. Rev. Fluid Mech.* **32**, 309–345.
- [3] MARBLE, F. E., HENDRICKS, G. J. AND ZUKOSKI, E. E. (1987). Progress toward shock enhancement of supersonic combustion processes. *AIAA 1987–1880*.
- [4] MENON, S. (1989). Shock-wave-induced mixing enhancement in scramjet combustors. *AIAA 1989–0104*.
- [5] BUDZINSKI, J. M., ZUKOSKI, E. E. AND MARBLE, F. E. (1992). Rayleigh scattering measurements of shock enhanced mixing. *AIAA 1992–3546*.
- [6] HERMANSON, J. C. AND CETEGEN, B. M. (2000). Shock-induced mixing of non-homogeneous density turbulent jets. *Phys. Fluids*, **12**(5), 1210–1225.
- [7] SHAU, Y. R., DOLLING, D. S. AND CHOI, K. Y. (1993). Organized structure in a compressible turbulent shear layer. *AIAA J.*, **31**(8), 1398–1405.
- [8] NUDING, J. R. (1996). Interaction of compressible shear layers with shock waves: an experimental study, part I. *AIAA 1996–4515*.
- [9] DRUMMOND, J. P. (1991). Mixing enhancement of reacting parallel fuel jets in a supersonic combustor. *AIAA 1991–1914*.
- [10] LU, P. J. AND WU, K. C. (1991). Mixing enhancement of reacting parallel fuel jets in a supersonic combustor. *Phys. Fluids A*, **3**(12), 3046–3062.
- [11] KIM, J. H., YOON, Y. AND JEUNG, I. S. (2003). Numerical study of mixing enhancement by shock waves in model scramjet engine. *AIAA J.*, **41**(6), 1074–1080.
- [12] GÉNIN, F. AND MENON, S. (2010). Studies of shock/turbulent shear layer interaction using large-eddy simulation. *Comput. Fluids*, **39**(5), 800–819.
- [13] REN, Y. X., LIU, M. AND ZHANG, H. X. (2003). A characteristic-wise hybrid compact-WENO scheme for solving hypersonic conservation laws. *J. Comp. Phys.*, **192**, 365–386.
- [14] ZHANG, H. Q., XUE, S. Y., WANG, B. AND WANG, X. L. (2009). Investigation on the shock-vortices interaction in a two-dimensional spatially developing supersonic mixing layer. In: *Asian-Pacific International Symposium on Aerospace Technology (APISAT-2009)*, Gifu, Japan.
- [15] GOEBEL, S. G., DUTTON, J. C., KRIER, H. AND RENIE, J. P. (1990). Mean and turbulent velocity measurements of supersonic mixing layers. *Experiments in Fluids*, **8**, 263–272.
- [16] BUTTSWORTH, D. R. (1996). Interaction of oblique shock waves and planar mixing regions. *J. Fluid Mech.*, **306**, 43–57.